Available online at www.sciencedirect.com
SCIENCE DIRECT®
Vision Research 45 (2005) 3454–3468
Vision Research
www.elsevier.com/locate/visres

Excitation mapping with the organic cation AGB^{2+}

Robert E. Marc [a,*], Michael Kalloniatis [b], Bryan W. Jones [a]

[a] John A. Moran Eye Center, 50 N Medical Drive, University of Utah School of Medicine, Salt Lake City, UT 84132, USA
[b] The Retinal Networks Laboratory, Department of Optometry and Vision Science, The University of Auckland, New Zealand

Received 16 June 2005; received in revised form 22 July 2005

Abstract

Excitation mapping is a method of visualizing the signaling history of neurons with permeant organic cations. It is compatible with high-resolution imaging, allowing concurrent visualization of all neuronal classes and their glutamate-gated excitation histories. Excitation mapping documents the stability and precision of neuronal signaling *within* a given neuronal class, arguing that single unit electrophysiological sampling accurately reflects neuronal diversity. We here review the theory of excitation mapping, provide methods and protocol links; outline imaging concepts; provide parametric data on the temporal range and physiological sensitivity of excitation mapping; and show that immunocytochemical methods for macromolecules are compatible with excitation mapping.

Keywords: Glutamate receptors; Immunocytochemistry; 1-Amino-4-guanidobutane; Agmatine; Imaging; Excitation mapping

1. Introduction

1.1. The theory of excitation mapping

Visualizing detailed maps of neuronal excitation is motivated by the complexity of vertebrate information processing assemblies such as the retina and hippocampus, where it is difficult to confidently assign physiological roles to morphologic classes of cells and more difficult to predict the behavior of neuronal populations. Further, electrophysiological profiling is complicated by non-uniform sampling, non-stationary behavior, and the high diversity of neuronal classes. Can an independent method be devised to corroborate this profiling? Imaging clearly offers better sampling, but what should be imaged and how can it be reconciled with single unit data? Older visualization methods such as radiolabeled 2-deoxyglucose transport autoradiography (described in Sokoloff et al., 1977) never achieved much success in retina due to poor resolution, prolonged analysis times, expense, and biohazards. Newer tools such as functional magnetic resonance imaging and calcium imaging still suffer from extremely poor spatial resolution, poor coverage, incompatibility with molecular markers for neuronal structure, or all three. Even when calcium imaging resolution is high, sample areas and depth-of-field become miniscule. Despite these limitations, calcium signals more directly reflect immediate synaptic activity than sugar transport because they often represent either ligand- or voltage-gated permeation events.

Following this line of thinking, other molecular species such as organic cations can also serve as permeation reporters. Tracking neuronal activity with organic cations is based on four basic concepts.

- Neurons decode and encode signals as ion currents through channels
- Channel permeation events generate large fluxes

* Corresponding author. Tel.: +1 801 585 6500; fax: +1 801 581 3357.
E-mail address: robert.marc@hsc.utah.edu (R.E. Marc).

0042-6989/$ - see front matter © 2005 Elsevier Ltd. All rights reserved.
doi:10.1016/j.visres.2005.07.025

- Many key cation channels are permeated by small organic reporter ions
- Small molecules can be haptenized to produce immunodetection reagents

If we employ organic cations reporters and channels as reporter conduits, will such signals be detectable in the primary fast signaling channels or "vertical" pathways of the retina served by ionotropic glutamate receptors (iGluRs) or metabotropic mGluR6 receptors? More specifically, since immunochemical detection methods for small molecules routinely span 0.1–10 mM (Marc, Murry, & Basinger, 1995), how quickly will permeant organic cations reach this range? Let us make the following simple but reasonable assumptions (see Hille, 2001 for an overview of concepts):

- A cubic cell with 10 μm edges and a volume of 1 pL
- A gated channel that transfers 10^6 ions s^{-1}
- An extracellular total permeant ion source of ≈150 mM
- An extracellular reporter ion representing 3% of the ion source (4.5 mM)
- A reporter permeation efficiency ≈0.4
- Complete probe trapping and no change in reversal potential

Under these conditions, it is simple to calculate that ≈830 channels are needed to raise the intracellular reporter level from 0 to 10 mM in 10 min. Assuming that glutamate receptor channel density is similar to nicotinic acetylcholine receptors, i.e., 10^4 μm^{-2} (Fambrough & Hartzell, 1972; Kunkel, Lee, & Stollberg, 2001), only a small fraction of the surface (≈0.08 μm^2 or 0.013%) would be required for permeation. Considering the small size of retinal bipolar cell dendrites, where the receptor patch at a single contact might be only ≈0.01 μm^2, eight active synapses would be sufficient. Thus, accumulation of immunodetectable levels of a reporter molecule is predicted by the basic attributes of known channels. Consistent with this, we will show that both exogenous and endogenous activation of iGluR channels are detectable and that there is a wide tradeoff between time and reporter concentration.

1.2. The reporters

Guanidinium ions and guanidinium analogues are a well-established family of organic channel permeant cations (Balasubramanian, Lynch, & Barry, 1995; Dwyer, Adams, & Hille, 1980; Larramendi, Lorente de No, & Vidal, 1956; Tasaki, Watanabe, & Singer, 1966). Their permeation is based on a very compact, resonance-stabilized cation: $C^+(NH_2)_3$. In the case of R-$C^+(NH_2)_2$ derivatives, efficient aldehyde trapping and hapten conjugation can be achieved if the R group contains reactive amino groups. Fig. 1 illustrates the atomic dimensions of hydrated sodium ions (Datta & Iyengar, 1991), the guanidinium cation (GU), 1-amino-4-guanidobutane (AGB or agmatine, the natural decarboxylation product of arginine), and L-2-amino-5-guanidino-pentanoate (ARG, arginine itself).

At physiological pH, AGB is a divalent cation due to its separately protonated guanidine and amino groups, while arginine is a *net* monovalent cation due to its additional carboxylate group. AGB likely behaves as a monovalent species in terms of initial microscopic channel interactions with the guanidinium head, but a divalent species in terms of macroscopic charge transfer. AGB is produced at extremely low levels in the mammalian nervous system and non-quantitative fluorescence imaging suggests that most of it is associated with very sparse neuronal terminals in cortex and spinal cord (Fairbanks et al., 2000). Indeed, there is a large literature on agmatine (AGB) as an endogenous imidazole receptor agonist (e.g., Raasch, Schafer, Chun, & Dominiak, 2001) and anti-inflammatory agent (Fairbanks et al., 2000), but the levels associated with these functions are clearly far below the millimolar values used in our flux experiments (see discussion in Marc, 1999b). On theoretical grounds at least, aldehyde-trapped intracellular guanidines should be quantitative reporters of time-integrated neuronal cation currents. This dependence on and compatibility with glutaraldehyde cross-linking in particular means that guanidine reporters could potentially provide high spatial resolution. If guanidine fluxes are predominantly coupled to signaling processes through neuronal depolarization, we can provisionally refer to such reporter detection as an *excitation history*.

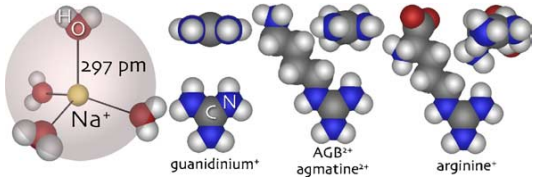

Fig. 1. Comparative sizes of guanidines and solvated Na ions. We assume a Pauling ionic radius of 97 pm for Na, a tetrahedrally bonded shell of four water molecules with Na-O bond lengths of 297 pm and H-O lengths of 99 pm. The series of guanidinium, 1-amino-4-guanidobutane (agmatine or AGB) and L-2-amino-5-guanidino-pentanoate (arginine) represents permeant species of increasing dimensions, but all are smaller or similar to the solvated Na ion in size. Each cation is shown in its largest and smallest rotational profile. Molecule shapes were generate as SMILES strings (see Weininger et al., 1989; also see Table 1 and www.daylight.com/smiles/f_smiles.html), translated to Brookhaven Protein Data Bank *.pdb format using the CORINA resource (www2.chemie.uni-erlangen.de/software/corina/index.html) and rendered with iMol v0.30 (www.pirx.com/imol).

1.3. Reporter detection

Guanidine flux visualization was first realized by Yoshikami (1981) by autoradiography of acetylcholine-gated [^{3}H]-AGB accumulation in frog sympathetic ganglion cells. This slow and demanding analytical method unfortunately hindered the exploration of organic cations as probes. An alternative strategy is immunodetection (Marc, 1999b). The tracking of small molecules with stereo- and regiospecific immunoglobulin G (IgG) reagents developed by Landsteiner (1945) has been exploited to a high degree of specificity by many laboratories. Most varieties of molecules can be haptenized and selective IgG production has been induced by haptens as exotic as C60 fullerenes (Chen, Wilson, Das, Coughlin, & Erlanger, 1998), as hydrophobic as steroids (Izhaky & Pecht, 1998), and as small as glycine (Yingcharoen, Rinvik, Storm-Mathisen, & Ottersen, 1989). Thus, it is of no surprise that molecules such as AGB and ARG elicit immune responses with high selectivity. Most importantly, immunodetection can track both exogenous and endogenous molecular signals at high spatial resolution.

The initial strategy of these experiments is simply incubation of isolated neural tissue (retina, in this case) for brief periods in physiological media containing AGB and selective activation of iGluRs by pharmacologic agents (Fig. 2). AGB influx is proportional to the channel permeability, AGB concentration and the driving force on the channel. As AGB is simply another cation in the stream, but is not extruded by Na-K ATPase, it continually accumulates. Because AGB is simply a permeant probe, it measures current through channels over time, not voltage over time. This means that it cannot directly report the integration of excitation and inhibition converging on a given cell. Indeed, converging inhibitory events that hyperpolarize the cell may increase the driving potential on the cation channel, slightly increasing the AGB current. This is an important point: AGB signaling reports an *excitation history* experienced by a cell due to flux through cation channels; this flux is not the summed excitation and inhibition voltages in that cell. This enables two kinds of experiments: (1) exogenous ligand application and (2) endogenous modulation of glutamate release. In this review, we will illustrate how to tune AGB concentration and

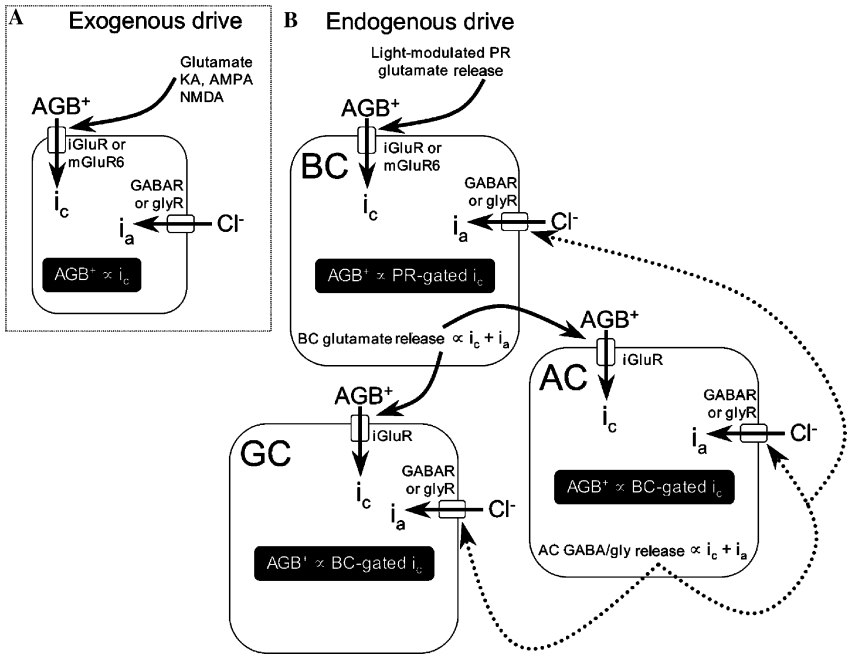

Fig. 2. AGB reporter schemes to detect (A) exogenous ligand-gated and (B) endogenous glutamate-gated cation currents in neurons. (A) Exogenous drive: a range of exogenous ligands activates cation-permeant iGluR or mGluR6 channels (KA, kainate; AMPA, α-amino-3-hydroxy-5-methylisoxazole-4-proprionic acid; NMDA, *N*-methyl-D-aspartate). Using a protocol shown to be insensitive to endogenous signals (5 mM AGB, 10 min incubations, Marc, 1999b), AGB signals are proportional to the total iGluR or mGluR cation currents (i_c). Anion currents (i_a) mediated by GABA and glycine receptors (GABAR, glyR) do not reduce this signal and may slightly increase it by increasing the driving force. (B) Endogenous drive: photoreceptor (PR) → bipolar cell (BC) → amacrine and ganglion cell (AC,GC) signaling chains depend on intrinsic glutamate release from either PRs or BCs. This can be detected by increasing incubation time or AGB concentration. Glutamate released by photoreceptors modulates AGB permeation into BCs. However, i_c and i_a (and other mechanisms) antagonistically sum to control release of glutamate from BCs, so that the AGB signal in ACs and GCs, in particular, reports the sum of presynaptic excitation and inhibition via glutamate release from BCs.

exposure time to preferentially detect only large signals such as direct exogenous activation of AGB permeation or to sensitively report endogenous glutamate-gated permeation events. In the latter, endogenous glutamate release from bipolar cells onto amacrine and ganglion cells is controlled by integrated excitation and inhibition. As AGB signals only report permeation through glutamate-activated channels, this means that downstream AGB signals in ganglion cells include a presynaptic or upstream *network history* (Fig. 2). Postsynaptic inhibition directly on the ganglion cell itself is undetected by AGB permeation, so the endogenous mapping method theoretically has the potential to segregate the effects of presynaptic amacrine cell → bipolar cell feedback from postsynaptic amacrine cell → ganglion cell feedforward.

2. Methods

2.1. The reporters

AGB is commercially available as a sulfate salt (1-amino-4-guanidobutane, $C_5H_{14}N_4 \cdot H_2SO_4$, CAS 2482-00-0) from Sigma–Aldrich and Fluka at 97–99% purity. The major contaminant is usually arginine, which is of no permeation consequence at low cation fractions. Similarly, brief elevations of sulfates to 3–10 mM appears to be of little physiological consequence (Marc, 1999b). However, longer exposures or higher AGB sulfate concentrations may be physiologically unacceptable, leading to partial anion channel block and failure of osmotic regulatory volume control (Petrunkina, Harrison, Ekhlasi-Hundrieser, & Töpfer-Petersen, 2004). A biionic solution of pure AGB sulfate thus triggers instability of horizontal cell membrane potentials, and this is corrected by using AGB chloride (Marc, Lembke, Solessio, & Rapp, unpublished data). AGB chloride is not commercially available but can be produced in the laboratory at reasonably high purity using either arginine decarboxylation at small-scales or $BaCl_2$ precipitation at large scales (Marc, unpublished data; see http://prometheus.med.utah.edu/~marclab/agb.html). AGB is normally stored at −20 °C, but we have found no evidence of degradation at least up to 30 days dry and 7 days aqueous solution storage at 4 °C. ARG, D-arginine (dARG) and guanidinium (GU) are commercially available as free acids or chloride salts. Saline solutions containing AGB, ARG, dARG or GU are made by adding the guanidines immediately before use without NaCl replacement for concentrations ⩽5 mM and with NaCl replacement otherwise. Guanidines are compatible with Hepes buffer and standard bicarbonate buffering; we have not evaluated Tris but do not recommend it. As shown in Table 1, the guanidinium groups of AGB, ARG, and dARG are cations at physiological pH (Gründemann, Hahne, Berkels, & Schömig, 2003; e.g., pK_a for the guanidine in arginine = 12.5). The primary amine has only a slightly lower pK_a (arginine and AGB $pK_{a2} \approx 9$) and, consequently, these molecules are net cations at physiological pH (AGB^{2+}, ARG^{+}, $dARG^{+}$). The data presented in this paper deal exclusively with AGB^{2+} detection.

2.2. The detectors

Rabbit polyclonal IgGs targeting AGB, AGR, and GU were produced using BSA–glutaraldehyde–amine conjugate immunogens (described in Marc et al., 1995). Anti-AGB IgGs licensed to Signature Immunologics (Salt Lake City, UT) are distributed by Chemicon International (Temecula, CA). Samples of any of these

Table 1
Cation channel reporters

Name	Code	IUPAC	Formula	Canonical SMILES (*isomeric)
Guanidinium^{+} MW 60.079 CID 32838 pK_a 12.6	GU	Diaminomethylideneammonium	CH_6N_3	C(=N)(N)N
L-Arginine^{+} MW 174.201 CID 232 pK_{a1} 12.5 pK_{a2} 9	ARG	L-2-Amino-5-guanidino-pentanoate	$C_6H_{14}N_4O_2$	C(CC(C(=O)O)N)CN=C(N)N
D-Arginine^{+} MW 174.201 CID 7170 pK_a values assumed same as L-arginine	dARG	D-2-Amino-5-guanidino-pentanoate	$C_6H_{14}N_4O_2$	*C(C[C=H](C(=O)O)N)CN=C(N)N
Agmatine^{2+} MW 130.192 CID 199 pK_{a1} 12.5 pK_{a2} 9	AGB	4-Aminobutyliminomethanediamine also 1-amino-4-guanidinobutane	$C_5H_{14}N_4$	C(CCN=C(N)N)CN

are available upon request from the Marc Laboratory at the University of Utah. These reagents are stored at −70 °C in serum and are stable indefinitely at 4 °C in a 100× concentrate working solution in 0.1 M phosphate buffer, pH 7.4, with 1% lyophilized goat serum as a protein carrier and 0.05% thimerosal. Full working solutions are stable for over 1 year at 4 °C. Anti-agmatine IgG have also been produced by the Reis laboratory (e.g., Fairbanks et al., 2000) at Weil-Cornell Medical College, NY. We have not evaluated them but presume them to behave similarly.

2.3. Tissue preparation and exposure

AGB in particular has been used in vitro for several tissue systems or in vivo via intravitreal injections for retinal mapping and aqueous exposure for fish olfactory system mapping (Edwards & Michel, 2002, 2003; Lipschitz & Michel, 2002; Sakata, Olson, & Michel, 2003). The in vitro protocol for retina has been described in detail (Marc, 1999a; Marc, 1999b) but involves mounting isolated retinal pieces ganglion-cell side down on cellulose triacetate filters as a support during tissue handling. A key strategy for performing incubations derives from our long experience with autoradiographic mapping of radiolabeled ligand transport and involves razor cutting filter-mounted retinas into small pieces prior to incubation, optimizing tissue use. Cut edges can evoke artifactual AGB signals (Marc, 1999b) as many retinal neurons and horizontal cells in particular are strongly coupled by gap junctions permeant to small molecules such as AGB or ARG. It is important to age cut pieces for 3–5 min in oxygenated, warm solutions to allow the cells to heal. Neural tissue must be also be handled with great care as guanidines present at immunodetectable extracellular levels can become fixed to the protein matrix of damaged cells (e.g., rods with broken outer segments) and can permeate glial cells that respond to local damage by activation of non-selective stretch sensitive cation channels (Marc, 1999b). Excitation mapping with guanidinium analogues thus reports all anomalies of tissue handing. Mouse tissues in particular are extremely sensitive and tissue handling or ligand-induced swelling can activate significant permeation into Müller cells (Rohrer et al., 2004). Labeling of broken cells could be reduced by rinsing prior to fixation, but this increases the chance of breaking more rods or stretch-activating MCs. Labeling of ruptured cells might be cleared by washing, but we argue that it is advantageous to clearly report the state of all cells.

Salines containing guanidinium analogues as reporters are inexpensive, so large numbers of samples or large retinal pieces are easily accommodated. Our routine method involves transferring each piece from its holding medium to small droplets (0.1–0.25 ml) of test medium containing activating ligands, antagonists, competitors, and reporters. Each piece is slipped into the droplet from the side, grasping only the filter with fine forceps, and an array of pieces concurrently incubated in a 60 ml disposable polystyrene dish with a loose cover continuous gas flow (95% O_2/5% CO_2) with bicarbonate-based Ames and 100% O_2 with Hepes Ames. The Kalloniatis laboratory uses Edwards medium (Edwards, Konnerth, Sakmann, & Takahashi, 1989) for rodent work. Immediately after incubation, fixative may be added directly to the droplets so that the tissues are well-stabilized before handling. Free amino acid and reporter signal trapping in isolated retinal samples is complete by 10 min using a standard 250 mM (2.5%) glutaraldehyde, 333 mM formaldehyde (1%) fixative (Marc, unpublished data).

2.4. Time and concentration

As originally shown in Marc (1999b), the accumulation of AGB at short times and high concentrations is not due to transporter activity, but rather channel permeation. Consequently, incubation time and AGB concentration should be inversely related over a wide range. The original selection of a basal 5 mM AGB level and 10 min incubation was motivated by the intent to track pharmacologically gated permeation events and these conditions were found to avoid significant endogenous signals. Raising the concentration to 25–50 mM confers greater sensitivity by increasing the fractional flux (see below) and it is possible to obtain strong signals in 60–120 s of AGB exposure in vitro. A key difference between exogenous ligand activated and endogenous glutamate signaling is the weaker efficacy of glutamate compared to kainate, AMPA, and NMDA. Increasing the concentration of AGB to 25 mM and/or the exposure time to 20 min thus amplifies detection by 2- to 10-fold in terms of net flux. As we will show, this enables detection of endogenous rod and cone activated signaling, as well as permeation through mGluR6-gated channels (also see Kalloniatis, Sun, Foster, Haverkamp, & Wässle, 2004). The ability to exchange time and concentration in the 1–100 mM range eliminates transporters as potential contributors to the flux signal (Gründemann et al., 2003; Marc, 1999b).

2.5. Fixation

The key to quantitative analysis of signaling with reporters is high-efficiency trapping and the dialdehyde fixative glutaraldehyde is ideal for both AGB trapping and visualization of small molecule signatures. While the routine trapping medium for AGB and small molecules is a variant of Karnovsky's medium, any properly buffered fixative with an appropriate level (10–250 mM) of glutaraldehyde will trap >85% of all endogenous amines. This is due to the dendrimer-like reactions that

most amines generate with glutaraldehyde as a core, and trapping runs until all amines are exhausted (see http://prometheus.med.utah.edu/~marclab/CMP_substrates.html). It is very important to include the monoaldehyde formaldehyde at 100–1000 mM, so that most of the matrix sites in tissue are decorated with a complex surface of large and small aldehyde links. This tremendously decreases background binding of IgGs. In general, we use: 250 mM glutaraldehyde (2.5%), 333 mM (1%) formaldehyde, 1 mM $MgSO_4$, and 3% sucrose in 100 mM phosphate buffer at pH 7.4. This fixative is incompatible with most IgGs targeting macromolecules. Kalloniatis and colleagues have shown that it is possible to use 1 mM (0.01%) glutaraldehyde (1 with 1332 mM 4%) formaldehyde and fluorescence detection to visualize AGB permeation and characteristic protein markers concurrently.

2.6. Sample preparation and visualization

Our computational molecular phenotyping (CMP) visualization technologies (Marc & Cameron, 2002) are based on thin section methods, which require resin-based embedding to achieve reliable thin 200–40 nm ultrathin serial sections. After fixation, tissues are dehydrated in graded methanols to acetone, infiltrated with epoxide resins and cured into blocs hard enough for electron beam stability but soft enough for thick section remounting methods. As retinas can be embedded as flat sheets, stacks of retinas can be assembled into sample arrays where a single thin section can contain samples from 1 to 10 experiments (Marc, 1999b; Marc, Liu, Kalloniatis, Raiguel, & van Haesendonck, 1990). Complete protocols for both resin embedding and stack fabrication are available at http://prometheus.med.utah.edu/~marclab/protocols.html. Samples are sectioned into serial arrays on 12-well HTC slides (Erie Scientific) for concurrent probing for a *basis set* of small molecules, including L-alanine (A), L-aspartate (D), L-glutamate (E), glycine (G), glutathione (J), L-glutamine (Q), taurine (τ), and GABA (γ,γ-aminobutyric acid): $A \cdot D \cdot E \cdot G \cdot J \cdot Q \cdot \tau \cdot \gamma$. This basis set is augmented by the excitation reporter AGB (B).

Probed CMP datasets are visualized with silver intensification, providing archival quantitative imagery (Kalloniatis & Fletcher, 1993; Kalloniatis, Marc, & Murry, 1996; Marc et al., 1990). Detailed protocols are available at the Marc laboratory web site, http://prometheus.med.utah.edu/~marclab/protocols.html along with descriptions of surface detection methods (http://prometheus.med.utah.edu/~marclab/CMP_substrates.html). Thin section images not previously published were captured at a calculated pixel scaling of 182 nm/pixel (40× planapochromatic oil immersion lens) with a QImaging QICAM IEEE-1394 12-bit cooled monochrome camera (www.qimaging.com) operated in the 8-bit mode. Illumination was controlled with a regulated Oriel power supply and no ripple or long-term drift was detectable. All images were tiled and aligned as previously described (Marc & Cameron, 2002) and *no filtering or contrast adjustment* was used prior to image analysis. Raw images are available at http://prometheus.med.utah.edu/~marclab/datasets.html.

Alternative methods include low glutaraldehyde–high paraformaldehyde methods and cryosectioning followed by double labeling with anti-AGB and other cell-specific anti-macromolecule markers (see Haverkamp & Wässle, 2000 for protocols). The key to this method is to increase anti-AGB concentrations about to compensate for the low trapping efficiency of the fixative. This necessarily renders AGB signaling somewhat qualitative, but this is nevertheless an important advance. The major protocol adjustments are AGB incubation at 25 mM, fixation in 1 mM glutaraldehyde and 1332 mM paraformaldehyde, and cryoimmunochemistry with five times higher anti-AGB IgGs.

2.7. CMP greyscale analysis

The main tools used for quantitative analysis of greyscale images are univariate histogramming and N-space cluster analysis, implemented as described in Marc et al. (1995) and Marc and Jones (2002). A tutorial on cluster analysis is available at http://prometheus.med.utah.edu/~marclab/CMP_analysis.html. The important concept underlying analysis of greyscale images is the fundamental trial-to-trial precision of the method across users and time, and the ability of greyscale images to encode roughly 2 log units of molecular concentration as pixel value (Marc & Jones, 2002). Our basic tool for univariate and multivariate histogram analysis is CellKit, an application developed in the Marc laboratory under the IDL image visualization language (www.rsinc.com) and operates in the freely distributed IDL VM environment. CellKit v2.2 is available from http://prometheus.med.utah.edu/~marclab/protocols_cellkit.html.

3. Results

3.1. Visualizing excitation history

Brief incubations ($\leqslant$10 min) in low concentrations of AGB ($\leqslant$5 mM) in the absence of any activating agent reveal no differential neuronal AGB signal in retina using standard silver visualization. However, activation with 100 μM KA (a saturating dose; see Marc, 1999b) is highly effective and evokes strong AGB entry into horizontal cells, bipolar cells, amacrine cells, and ganglion cells (Fig. 3). Importantly, all horizontal cells of a given class (e.g., type B) behave identically (Marc, 1999a, 1999b), which provides a basis for understanding variation in signaling in more complex populations of amacrine

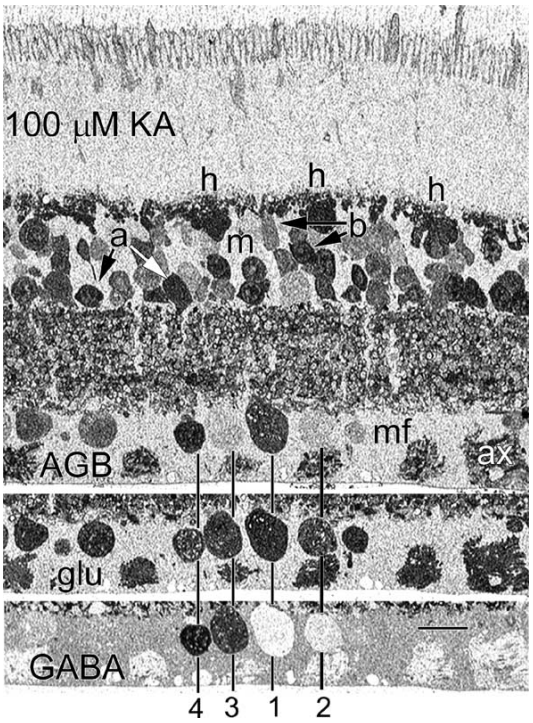

Fig. 3. AGB signals isolated in rabbit retina after incubation with 5 mM AGB + 100 μM KA. Endogenous glutamate (glu) and GABA signals in the ganglion cell layer are shown as registered strips from serial sections with selected cell classes marked by vertical lines with labels below: 1, E+ ganglion cells with strong AGB responses; 2, E+ ganglion cells with weak signals; 3, E+/γ + ganglion cells with weak AGB signals; 4, γ + starburst amacrine cells with strong signals. ax, Ganglion cell axon bundles, m Müller cells, mf Müller cell end feet. Amacrine (a) and bipolar (b) cells also display a range of responses while horizontal (h) cells all show the same response. Scale bar, 20 μm. Reproduced from Marc (1999b) by permission of Wiley Interscience.

and ganglion cells. If a single neuronal class behaves consistently, cells with different grey level responses are likely to be biologically different classes. As 100 μM KA should be saturating for all AMPA receptor subtypes, the presence of cells with weak AGB signals implies that either few channels are expressed per cell or the unitary conductance of each assembly is low, or both. We demonstrated that this argument is consistent with the labeling behavior of individual ganglion cell classes (Marc & Jones, 2002). The differential *concurrent* activation of different neuronal populations by a single application of an agonist can be documented by correlating multiple molecular signals from the basis set with reporter signals of individual cells in registered serial sections (Fig. 3). Specifically, γ+ starburst amacrine cells and large E+ ganglion cells show strong AGB signals in response to 100 μM KA, whereas certain medium-sized ganglion cells and some dual E+/γ+ ganglion cells demonstrate little or no induced response. We have shown that the latter belong to a class of ganglion cells (Marc & Jones, 2002, class 12) that likely correspond to a set of sluggish transient ganglion cells. In addition, it is clear that only a subset of bipolar cells is activated by KA (Marc, 1999a; Rohrer et al., 2004) and these, by definition, should be OFF bipolar cells.

Do polysynaptic effects confound these pharmacologic signals? While it is certain that KA-activated bipolar cells will release glutamate and must trigger permeation events via both AMPA and NMDA receptor channels in target cells, and that this additional signal should be superimposed on the intrinsic KA-activated AMPA receptor signal, can we see that increment with brief (10 min) exposures and low (5 mM) levels of AGB? Might not nicotinic pathways corrupt the datasets? Six kinds of experiments reported in Marc (1999b) argue not.

(1) Endogenous glutamate signaling is not detectable with this brief protocol.
(2) Exogenous glutamate signaling is not detectable without blockade of glutamate transporters (i.e., blocking presynaptic and glial clearance of glutamate). Thus, it is unlikely that KA-evoked glutamate release could be differentially detected.
(3) KA and NMDA activation generate very different laminar patterns of signaling in the inner plexiform layer. If endogenous glutamate release were a significant source of AGB signal, KA stimulation should mimic NMDA response patterns. It does not.
(4) NMDA antagonists do not change the KA pattern.
(5) KA agonists *do* change the NMDA pattern, but only by reducing its peak value. This demonstrates that endogenous occupancy of the AMPA receptor is likely the key mechanism overcoming voltage-dependent NMDA block.
(6) Activation of nicotinic receptors with carbachol, epibatidine or acetylcholine does not generate any AGB signal.

Presuming the ligand-driven responses to be uncontaminated by endogenous networks, it follows that response diversity can be exploited to discover and display physiological classes of neurons. By sectioning in the horizontal plane of of cell somas such as the ganglion cell layer (Fig. 4), it is possible map to concurrent responses of a large cohort of neurons and extract their molecular signatures using CMP and a basis set of probes. These data demonstrate that each single ganglion cell class possesses a characteristic permeation response to AMPA receptor activation. We argue that this fundamental response strength is partially responsible for the differential spiking patterns of ganglion cells: that cells with large responses are brisk and those with weak responses are sluggish variants (Marc & Jones, 2002).

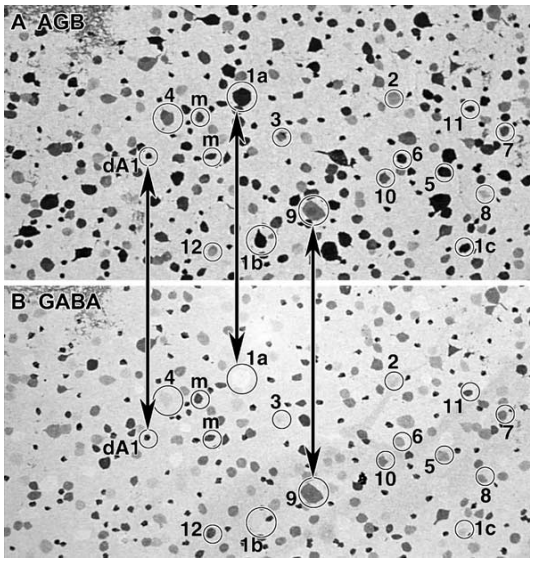

Fig. 4. Two images (A, AGB; B, GABA) from a 7-dimensional molecular series through the rabbit ganglion cell layer after activation with 25 μM AMPA. These two panels show correlated signals of 15 classes of resident neurons in the ganglion cell layer, including γ+ displaced starburst amacrine cells (dA1) and 14 classes of ganglion cells. Two misplaced amacrine cells (m) are also indicated. Each image is 885 μm in width. Excerpted from Marc and Jones (2002) by permission of the Society for Neuroscience.

3.2. Greyscale analysis

The data in Fig. 4 provide an ideal opportunity to illustrate the quantitative nature of the silver-based visualization method and CMP. Concurrent univariate and bivariate histograms of AGB and GABA signals of ganglion cell classes 1, 3, 5, and 12 are shown in Fig. 5 along with the entire neuronal cohort signal histograms. The use of quantitative grey level immunocytochemical data allows extremely powerful segmentation of images, especially when higher dimensions of data are available. The univariate AGB signals of all four classes represent different distributions with very high significances ($p < 0.0001$ for any pair using parametric models). However, one cannot extract the classes from a single image because the distributions overlap. For example, class 12 overlaps class 3 in AGB response and class 5 over laps 1. Similarly, classes 1, 3, and 5 overlap in GABA content. By considering their *bivariate* signals, however, it is clear that class 12 exists in a molecular space that is always separate from the other three, and that despite their univariate overlaps, classes 1, 3, and 5 each occupy a unique portion of signal space. By extending this kind of analysis to three and more molecular dimensions, further power in separability is acquired (see Marc & Jones, 2002).

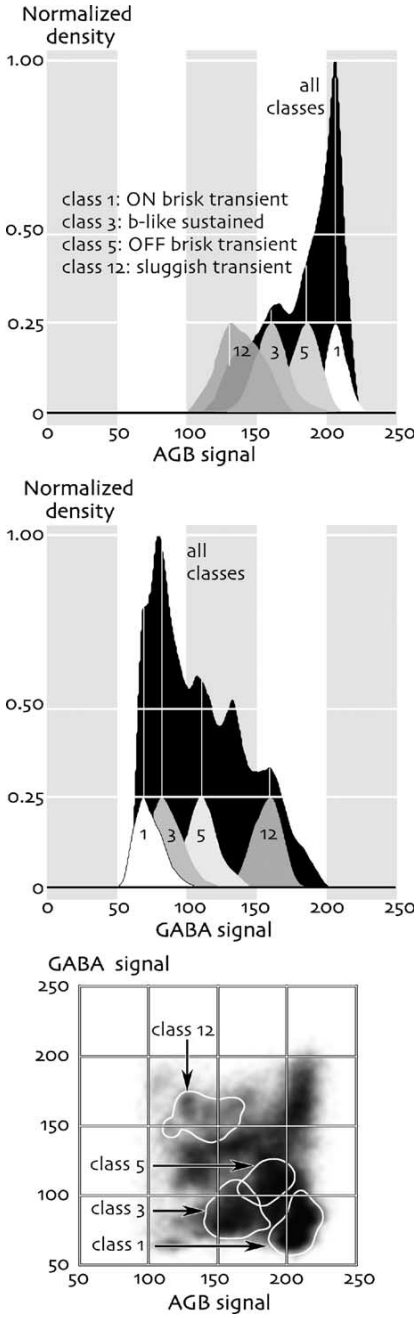

Fig. 5. Peak-normalized AGB and GABA univariate and bivariate signal strength histograms for a sample of over 600 ganglion cells. The abscissa is the 8-bit AGB or GABA grey level intensity (0–255) and the ordinate is normalized probability density. Top: the histogram for all cells in the ganglion cell layer is shown in black. The underlying histograms for classes 1, 3, 5, and 12 (see Fig. 4) are arbitrarily normalized to 0.25 to visualize their different positions along the AGB signal axis. Class 1 cells are the most AMPA-responsive. Middle: the same sets of cells visualized as histograms of GABA signals. Bottom: the same sets of cells visualized as a bivariate AGB vs GABA density histogram with the borders of the 95% level skirts of each class outlined in white. Bivariate clustering shows better separability than univariate analysis.

3.3. Exchanging time and AGB concentration

Our initial analyses of AGB permeation at 5 mM for 10 min showed that retinal OFF bipolar cells were selectively activated by AMPA and KA; that ON bipolar cells were apparently not permeant to AGB or at least not detectable (Marc, 1999a, 1999b). By increasing either the exposure time or the concentration of however, it became clear that the non-selective cation channels of ON bipolar cells were AGB-permeant and that this endogenous signaling could be blocked by 2-amino-4-phosphonobutyrate (AP4, Kalloniatis et al., 2004). This implies that increased flux is required to detect ON bipolar cells, and that the product of the AGB permeability, unitary conductance and density channels gated of by the mGluR6 receptors is significantly smaller than for AMPA or NMDA receptors. It further argues that AGB behaves as a classic permeant cation, showing little detectable channel saturation, and is further evidence that AGB enters cells by channel permeation and not transport.

We have parametrically explored the temporal and sensitivity limits of excitation mapping. A major strength of the CMP method is the ability to stack multiple samples into a single bloc and probe them concurrently. Isolated rabbit retinal samples mounted on filter chips were incubated in parallel for varied times in different AGB concentrations while activated in 50 μM KA and then concurrently probed as stacks. Fig. 6 shows the extent of response detection achieved at low and high concentrations. As originally described in Marc (1999a), 5 mM AGB at 10 min is a highly sensitive regime and produces extremely strong responses in all superclasses of retinal neurons. Even so, strong responses are detectable even at 2 min of incubation and the responses of the most sensitive neurons in the retina, starburst amacrine cells, are evident at 60 s. One robust measure of retinal responsivity to pharma-

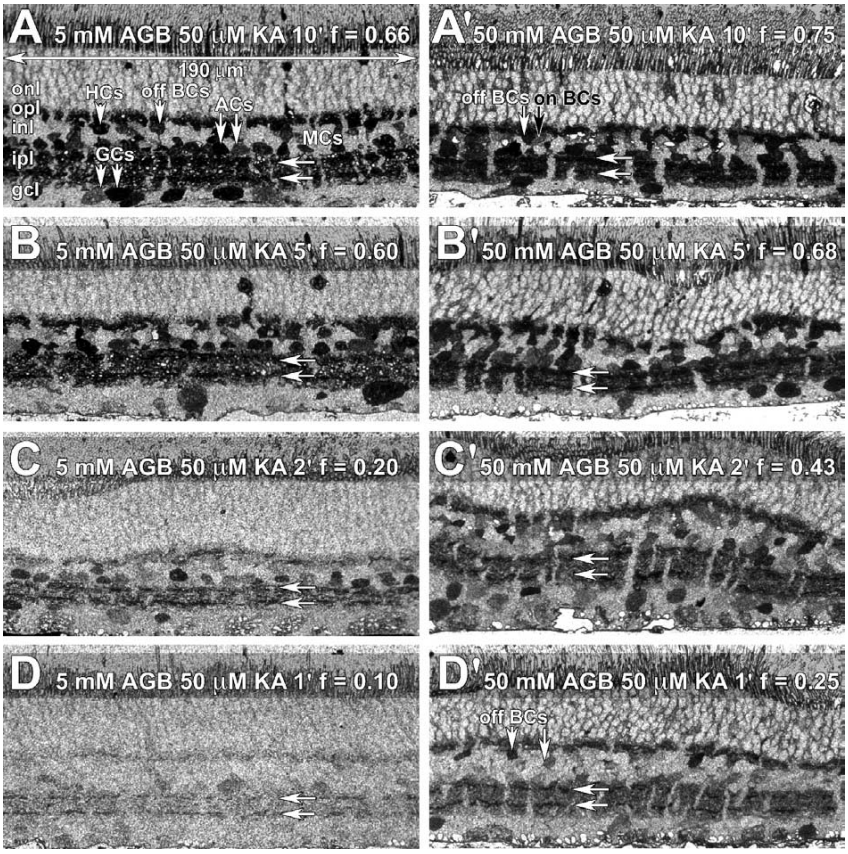

Fig. 6. The time course of AGB permeation at high and low AGB levels. (A–D) Matched retinal samples incubated under 50 μM KA activation in 5 mM AGB for 1, 2, 5, and 10 min. (A′–D′) Matched retinal samples incubated under 50 μM KA activation in 50 mM AGB for 1, 2, 5, and 10 min. (A) Indexes responsive horizontal (HCs), OFF bipolar (off BCs), amacrine (ACs), and ganglion (GCs) cells. Müller cells (MCs) maintain the same background signal at all activation levels. Horizontal arrows mark the stratification levels of starbust amacrine cells. In each panel, the fractional response (f) of the inner plexiform layer (ipl) is shown (see Marc, 1999b for calculation). At high AGB levels (50 mM, A′), ON bipolar cells begin to show endogenous permeation in vitro. Each panel is 190 μm wide. Other abbreviations: onl, outer nuclear layer; opl, outer plexiform layer; inl, inner nuclear layer; gcl, ganglion cell layer.

cologic activation is the fractional response (f) introduced in Marc (1999b). This measure is substantially different from the total greyscale signal (cf. Sun, Rait, & Kalloniatis, 2003). The fractional response is an area measurement that asks: "What fraction of the neuropil has been activated above a specified detection threshold." This allows direct comparison of total responsivity among retinas, even though individual cell classes have different saturation levels to a ligand. Thus, a saturating KA fractional response is in the range of 0.55–0.70 for 5 mM AGB at long times and progressively less a short times. Though this is a non-linear measure, it nevertheless demonstrates that 50 mM AGB at only 60 s generates a KA activation signal that is much greater than 5 mM can achieve in 2 min. These data show that excitation mapping has a wide latitude and that AGB concentration and time are readily exchangeable.

Importantly, the ligand activated AGB permeation into retinal neurons is an increasing function of AGB concentration and even at 50 mM AGB, representing about 1/3 of all permeant cations, the flux appears non-saturating (Figs. 7 and 8). This is consistent only with the behavior of a channel and completely excludes transporters as possible entry routes. Furthermore, it demonstrates that AGB selectively tracks excitation history over a wide range of probe levels. This sets the stage for using AGB as an in vivo probe and a probe of endogenous signaling, which we have achieved in several formats. These are beyond the scope of this review, but should encourage other investigators to explore the use of this probe. The important message is that AGB map-

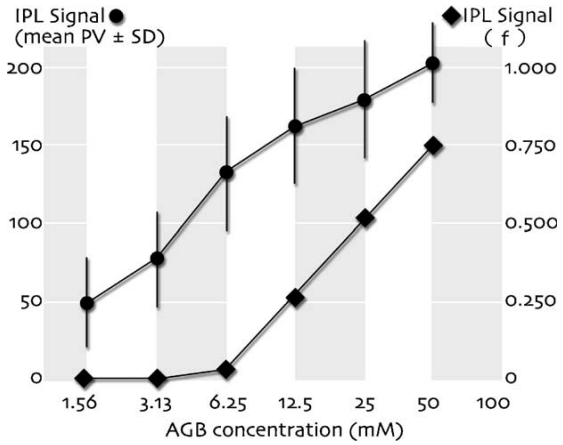

Fig. 8. Increasing grey level signal as mean pixel value (PV = dots) ±1 standard deviation (*SD*) and fractional response (f = diamonds) as a function of AGB concentration for a constant 4 min activation with 50 μM KA. These data were abstracted from the retinas in Fig. 6 over 0.5–1 mm of length of retinal tissue, each spanning $>10^3$ retinal neurons. PV was measured as the mean histogram signal for the isolated IPL. PV is more sensitive than FR, but both show increasing flux as a function of AGB concentration, showing that the signal is consistent solely with a permeation process.

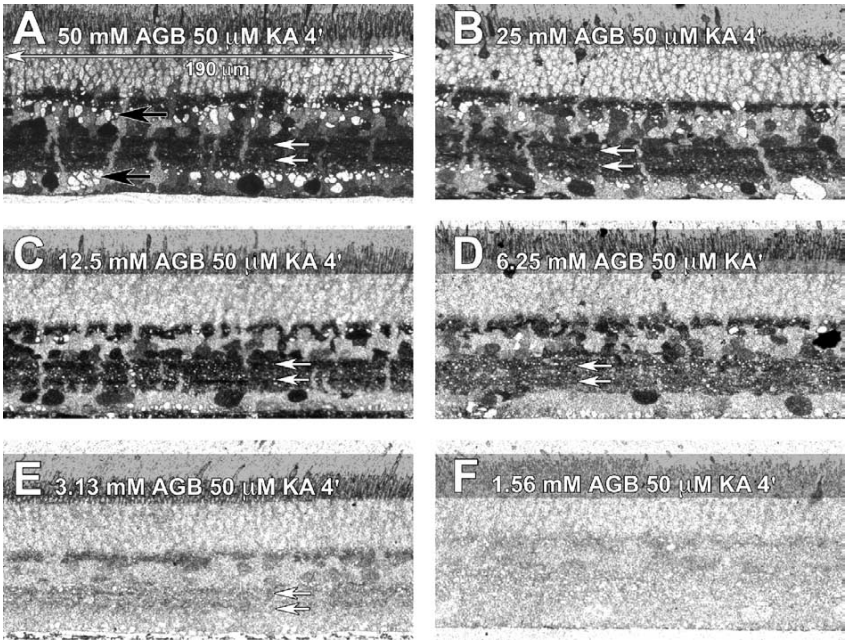

Fig. 7. The concentration-dependence of AGB permeation. A single rabbit retina was cut into chips and each concurrently incubated for 4 min in 50 μM KA and serial 2-fold dilutions of AGB ranging from 50 to 1.56 mM (A–F). As in Fig. 6, white arrows mark the starburst amacrine strata. This sample showed some Müller cell swelling at the highest concentrations, but this is a variable effect and may be due to mechanical stimulation (see Marc, 1999b).

ping is very tolerant of diverse conditions and can be tuned to high sensitivities with high concentrations of AGB, while remaining sensitive at low concentrations that do not perturb ionic balances. Indeed, it should be emphasized that AGB use is not without risk, as it appears to be an inhibitor of Na-K ATPase through antagonism at the Na binding site (Or, David, Alla Shainskaya, Tal, & Karlishs, 1993) and is an inhibitor of NO synthase (Feng, Piletz, & LeBlanc, 2002; Galea, Regunathan, Eliopoulos, Feinstein, & Reis, 1996). But since both of these actions require AGB to permeate and accumulate to significant levels, it is likely that they play no major role in short-term response patterns.

3.4. Endogenous signal mapping

The greyscale sensitivity and enhanced detectivity with increased AGB concentration gives AGB the potential for mapping endogenous glutamate signaling, which induces much smaller signals than exogenous pharmacologic drive. But since we can increase sensitivity 2- to 3-fold by using longer incubations, carefully controlled lighting conditions routinely trigger AGB permeation in *both* ON and OFF bipolar cells. This response pattern is only elicited successfully in on-choroid preparations. Isolated retinas show little activity even after 20 min in 5 mM AGB. Fig. 9 shows excitation mapping in a dark-adapted on-choroid rabbit retina driven in vitro with mesopic (1.84 quanta s^{-1} μm^{-2}) 550 nm 2 Hz^2-wave light for 20 min in the presence of 5 mM AGB. This stimulus flux is about a log unit above threshold for most cone ON bipolar cells and a log unit below that of the least sensitive cone ON bipolar cells (see Fig. 6 in Pang, Gao, & Wu, 2004). All B-type horizontal cells are homogeneously light responsive, while each bipolar cell cohort is multimodal

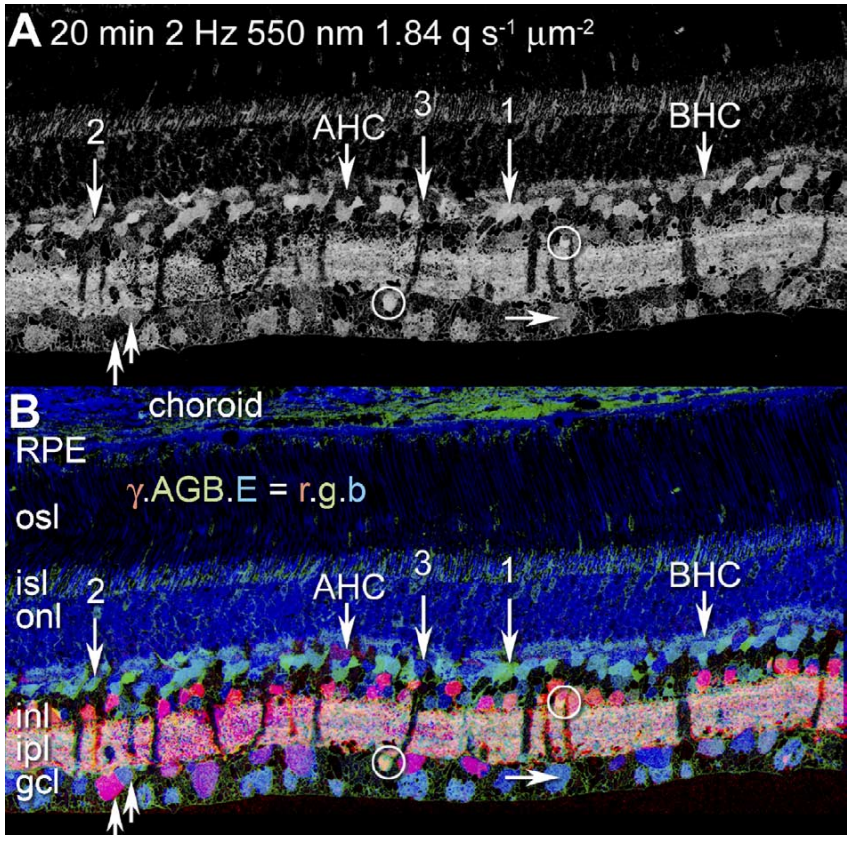

Fig. 9. Light-driven AGB signals in the in vitro rabbit retina with intact RPE and choroid. The retina was driven 20 min with 1.84 quanta s^{-1} μm^{-2} 550 nm 2 Hz^2-wave light (50% duty cycle) in Ames medium with 5 mM AGB. The top panel (A) shows the AGB response alone (as an inverted, brightness-scaled image) and the bottom (B) is a $\gamma \cdot AGB \cdot E = rgb$ mapping. Strong permeation was activated in a great range of target neurons including all rod bipolar cells, cone OFF bipolar cells and most but not all cone ON bipolar cells and not type A horizontal cells. Cell classes were defined by CMP signatures (see Marc, 1999a; Marc and Jones, 2002). Arrows denote instances of the three modes of cone ON bipolar cell responses. Mode 1 is a highly responsive cohort, mode 2 shows moderate responses and mode 3 shows no responses. ON and OFF starburst amacrine cells are circled, which have strong mesopic light responses. Ganglion cell signals were weaker and varied by class (upward arrows) with α-like cells (horizontal arrows) showing mid-range responses.

(Fig. 10). Rod bipolar cell light responses are not quantitatively distinguishable from those of most cone-driven OFF bipolar cells and they collectively form modes 2 and 3 of the light-response histogram. A sparse set of highly responsive bipolar cells appears give the strongest signals and form mode 1. We believe these are cone-driven OFF bipolar cells, but verifying this will require further analysis with horizontal sections. Cone-driven ON bipolar cells, identified by their glycine content (e.g., Marc, 1999a), are clearly segregated into three modes under 550 nm light: high, medium and unresponsive. It is, tempting to presume that mode 3 represents cells driven by blue cones, but that remains to be seen. Starburst amacrine cells remain the most sensitive of the inner retinal neurons. We had previously shown that they were the most responsive amacrine cell when driven by AMPA and kainate (Marc, 1999a, 1999b, Marc & Jones, 2002), but this demonstrates that they are also likely the most sensitive when driven by endogenous glutamate release from cone bipolar cells as well. Finally, endogenous ganglion cell responses are the weakest and most diverse, consistent with the idea their serial light-activated → glutamate-gated currents may reflect presynaptic integration at the level of bipolar cell terminals. We view this as a major tool for parsing endogenous responses in entire populations.

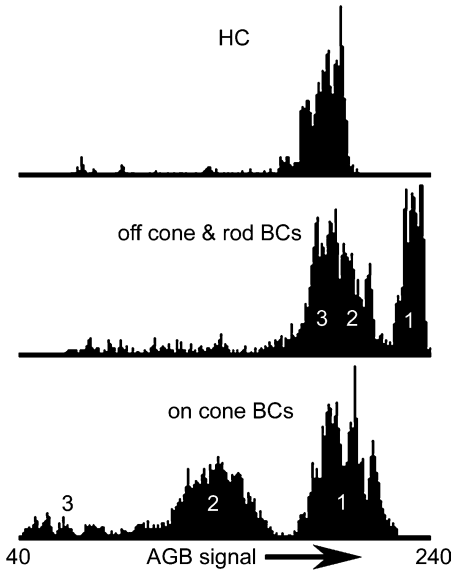

Fig. 10. Three histograms of cellular light-driven responses determined by AGB mapping. The ordinate is the probability density of finding a response at a given AGB signal (abscissa) based on an 8-bit intensity scale (0–255), truncated to a 40–240 grey level range. Cells with a value of 40 are at a "background" signal equivalent to the Müller cell signal. Cells above 40 and approaching 240 represent a range of increasingly stronger responses to the stimulus. The data were derived from Fig. 9. Top: type B HCs show good responses to 550 nm light, but are weaker than some OFF and ON bipolar cells. Middle: the OFF and rod bipolar responses cannot be separated (modes 2 and 3), but subpopulations can be identified, including a highly responsive group (mode 1). Bottom: cone-driven ON bipolar cells are the most distinctive, segregating into at least three major cohorts: poorly responsive (mode 3), moderately responsive (mode 2) and highly responsive (mode 1).

3.5. Combining excitation mapping with macromolecule immunocytochemistry

A major limitation in the use of excitation mapping has been the strong dependence of AGB trapping on glutaraldehyde, which prevents the use of antibodies against a range of interesting macromolecules that serve as useful classifiers of neurons (Haverkamp & Wässle, 2000). Kalloniatis and colleagues have developed protocols that enable the use of AGB with such probes (see Section 2). Mouse retinas incubated 5 min in Edwards medium (Edwards et al., 1989) with 25 mM AGB were activated with KA or NMDA and the colocalization of activation mapped onto calretinin+ or calbindin+ neurons by double-label immunocytochemistry (Fig. 11). While the fine-scale differential responses of individual neurons cannot be analyzed properly in such thick sections due to superposition of signals, selective activation can be achieved. For example, at 5 μM KA, OFF bipolar cells and some sets of amacrine cells and ganglion cells are readily detected (Fig. 11A), but this dose is below threshold for horizontal cells (Marc, 1999b). Several classes of calretinin+ amacrine cells (red channel) are present, but they have rather weak responses to KA. Increasing the KA dose to 50 μM generates robust signals that superimpose nicely on calbindin+ horizontal cell somas as a bright orange-yellow summed signal. Finally, NMDA selectively activates neurons of the proximal retina (Kalloniatis et al., 2004; Marc, 1999a, 1999b; Sun et al., 2003), and calbindin+ horizontal cells lack any AGB signal, while the calbindin+ amacrine cell cohort is strongly activated by NMDA. This improved immunocytochemical protocol offers the opportunity to explore AGB signaling with a number of new probes.

4. Discussion

Excitation mapping offers new opportunities to assay the behaviors of populations of neurons and retinal neurons in particular. We have yet to thoroughly explore all of the applications of the method, but we are certain that it is a useful tool for analyzing pharmacologic data, and may even serve as a screening method for drug leads. The ability to detect both ligand-activated and synaptically modulated signaling offers tremendous opportunities to dissect pathways and characterize the fundamental signaling attributes

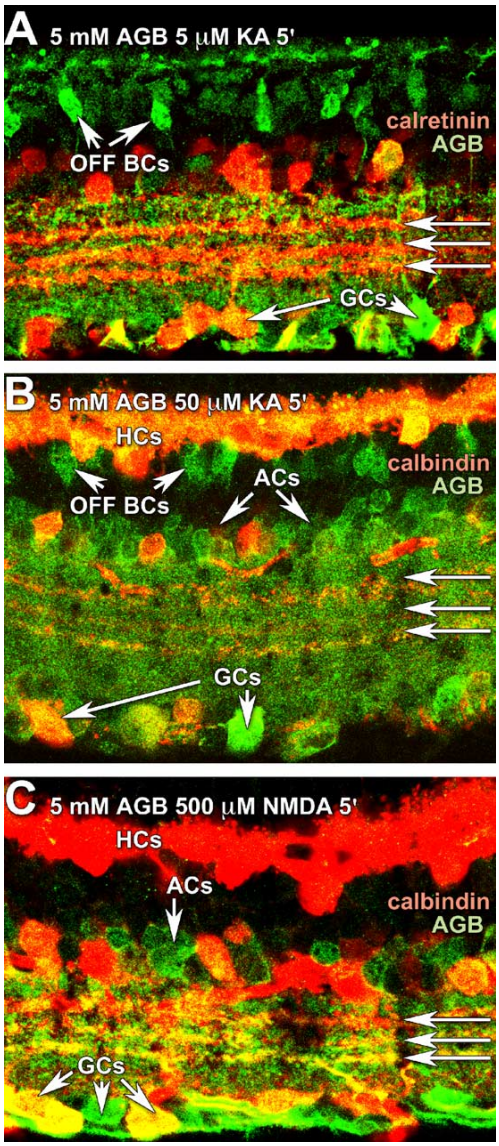

Fig. 11. Concurrent visualization of calcium binding proteins and iGluR signaling using the Kalloniatis method (see text). In each panel, fluorescent imaging maps a calcium binding protein as the red channel and ligand-induced AGB signals as the green channel. (A) Mouse retina incubated in 5 mM AGB + 5 μM KA for 5 min, resulting in strong activation of OFF bipolar cells and amacrine and ganglion cell neurites throughout the IPL. Neurons projecting to a characteristic triple band of ganglion cell rich neurites (see Wässle, 2004) are labeled with anti-calretinin IgGs and visualized with Alexa conjugated secondary IgGs (Molecular Probes). (B) Increasing the KA level to 50 μM recruits horizontal cells (yellow + red signal) into the response spectrum along with OFF bipolar cells and most amacrine and ganglion cells. The horizontal cells are labeled with anti-calbindin IgGs and visualized with Alexa conjugated secondary IgGs. (C) Switching to 500 μM NMDA selectively activates amacrine and ganglion cell subsets, especially (but not exclusively) those that project to the ganglion cell rich triplet bands. Horizontal cells are not activated. The horizontal cells are labeled with anti-calbindin IgGs and visualized with Alexa conjugated secondary IgGs.

of complex populations of neurons (Kalloniatis et al., 2004; Marc, 1999a, 1999b; Marc & Jones, 2002; Rohrer et al., 2004). We now know that all glutamate-driven cells, including ON bipolar cells, possess channels permeant to AGB. In particular, the endogenous AGB permeation of ON bipolar cells requires the participation of an AP4-sensitive mechanism, arguing that the mGluR6 transduction pathway is being probed (Kalloniatis et al., 2004). Future applications of AGB mapping include screening the emergence of functional pathways in development and tracking the disassembly of retinal signaling in disease (Marc, Jones, Watt, & Strettoi, 2003).

We have successfully used intravitreal AGB injections in fishes, rabbits, and rodents to map endogenous activity and the patterns are consistent with summed iGluR and mGluR6 mediated signaling, but these unpublished data are beyond the scope of this review. Even so, it is clear that it will also be possible to track endogenous activity under controlled lighting conditions, in genetic models of function or disease, and under systemic drug treatments. We also know that AGB mapping reports iGluR signaling in hippocampal slices (Takahashi, Jones, & Marc, 2004), zebrafish central pathways (Edwards & Michel, 2002, 2003; Sakata et al., 2003) and olfactory cell transduction (Lipschitz & Michel, 2002; Steullet, Cate, Michel, & Derby, 2000). Combined with new evidence that AGB is partially permeant to the blood–brain barrier (Piletz, May, Wang, & Zhu, 2003), this offers the likelihood that in vivo CNS excitation mapping can also be achieved in the short-term.

More concretely, we here show that the excitation mapping method has great latitude; that, as expected of a channel-mediated process, time and concentration can be interchanged. Increasing AGB concentration confers greater sensitivity and large signals are generated more rapidly. Finally, by varying some key experimental parameters, it is now possible to superimpose excitation histories characteristic of selective AMPA or NMDA channel activation on structural maps acquired by conventional macromolecule immunocytochemistry and fluorescence detection.

Acknowledgments

This work was supported by NEI Grants EY002576 and EY015128 (RM), Research to Prevent Blindness funding to the University of Utah, and a grant from the Health Research Council of New Zealand 02/226 (MK). MK holds a professorship funded, in part, by the Robert G. Leitl estate. Conflict-of-Interest: R.M. is a principal of Signature Immunologics.

References

Balasubramanian, S., Lynch, J. W., & Barry, P. H. (1995). The permeation of organic cations through cAMP-gated channels in mammalian olfactory receptor neurons. *Journal of Membrane Biology, 146*, 177–191.

Chen, B. X., Wilson, S. R., Das, M., Coughlin, D. J., & Erlanger, B. F. (1998). Immunology antigenicity of fullerenes: Antibodies specific for fullerenes and their characteristics. *Proceedings of the National Academy of Sciences of the United States of America, 95*, 10809–10813.

Datta, S. N., & Iyengar, S. S. (1991). Semi-empirical Hartree-Fock calculations on the mechanism of enniatin B mediated transport of sodium ions. *Chemistry and Physics Letters, 183*, 491–498.

Dwyer, T. M., Adams, D. J., & Hille, B. (1980). The permeability of the endplate channel to organic cations in frog muscle. *Journal of General Physiology, 75*, 469–492.

Edwards, F. A., Konnerth, A., Sakmann, B., & Takahashi, T. (1989). A thin slice preparation for patch clamp recordings from neurones of the mammalian central nervous system. *Plugers Archives, 414*, 600–612.

Edwards, J. G., & Michel, W. C. (2002). Odor-stimulated glutamatergic neurotransmission in the zebrafish olfactory bulb. *Journal of Comparative Neurology, 454*, 294–309.

Edwards, J. G., & Michel, W. C. (2003). Pharmacological characterization of ionotropic glutamate receptors in the zebrafish olfactory bulb. *Neuroscience, 122*, 1037–1047.

Fairbanks, C. A., Schreiber, K. L., Brewer, K. L., Yu, C.-G., Stone, L. S., Kitto, K. F., Nguyen, H. O., Grocholski, B. M., Shoeman, D. W., Kehl, L. J., & Regunathan, S. (2000). Agmatine reverses pain induced by inflammation, neuropathy, and spinal cord injury. *Proceedings of the National Academy of Sciences of the United States of America, 97*, 10584–10589.

Fambrough, D. M., & Hartzell, H. C. (1972). Acetylcholine receptors: number and distribution at neuromuscular junctions in rat diaphragm. *Science, 176*, 189–191.

Feng, Y.-Z., Piletz, J. Z., & LeBlanc, M. H. (2002). Agmatine suppresses nitric oxide production and attenuates hypoxic-ischemic brain Injury in neonatal rats. *Pediatric Research, 52*, 606–611.

Galea, E., Regunathan, S., Eliopoulos, V., Feinstein, D. L., & Reis, D. J. (1996). Inhibition of mammalian nitric oxide synthase by agmatine, an endogenous polyamine formed by decarboxylation of arginine. *Biochemistry Journal, 316*, 247–249.

Gründemann, D., Hahne, C., Berkels, R., & Schömig, E. (2003). Agmatine is efficiently transported by non-neuronal monoamine transporters extraneuronal monoamine transporter (EMT) and organic cation transporter 2 (OCT2). *The Journal of Pharmacology and Experimental Therapeutics, 304*, 810–817.

Haverkamp, S., & Wässle, H. (2000). Immunocytochemical Analysis of the Mouse Retina. *Journal of Comparative Neurology, 424*, 1–23.

Hille, B. (2001). *Ion channels of excitable membranes* (3rd ed.). Sunderland, MA: Sinauer, p. 722.

Izhaky, D., & Pecht, I. (1998). What else can the immune system recognize? *Proceedings of the National Academy of Sciences of the United States of America, 95*, 11509–11510.

Kalloniatis, M., & Fletcher, E. L. (1993). Immunocytochemical localization of the amino acid neurotransmitters in the chicken retina. *Journal of Comparative Neurology, 336*(2), 174–193.

Kalloniatis, M., Marc, R. E., & Murry, R. F. (1996). Amino acid signatures in the primate retina. *Journal of Neuroscience, 16*(21), 6807–6829.

Kalloniatis, M., Sun, D., Foster, L., Haverkamp, S., & Wässle, H. (2004). Localization of NMDA receptor subunits and mapping NMDA drive within the mammalian retina. *Visual Neuroscience, 21*, 587–597.

Kunkel, D. D., Lee, L. K., & Stollberg, J. (2001). Ultrastructure of acetylcholine receptor aggregates parallels mechanisms of aggregation. *BMC Neuroscience*(5). doi:10.1186/1471-2202-1182-1119.

Landsteiner, K. (1945). In *The specificity of serological reactions* (pp. 450). Boston: Harvard University Press.

Larramendi, L. M., Lorente de No, R., & Vidal, F. (1956). Restoration of sodium-deficient frog nerve fibres by an isotonic solution of guanidinium chloride. *Nature, 178*, 316–317.

Lipschitz, D. L., & Michel, W. C. (2002). Amino acid odorants stimulate microvillar sensory neurons. *Chemical Senses, 27*, 277–286.

Marc, R. E. (1999a). Kainate activation of horizontal, bipolar, amacrine, and ganglion cells in the rabbit retina. *Journal of Comparative Neurology, 407*(1), 65–76.

Marc, R. E. (1999b). Mapping glutamatergic drive in the vertebrate retina with a channel-permeant organic cation. *Journal of Comparative Neurology, 407*(1), 47–64.

Marc, R. E., & Cameron, D. A. (2002). A molecular phenotype atlas of the zebrafish retina. *Journal of Neurocytology, 30*, 593–654.

Marc, R. E., & Jones, B. W. (2002). Molecular phenotyping of retinal ganglion cells. *Journal of Neuroscience, 22*, 412–427.

Marc, R. E., Jones, B. W., Watt, C. B., & Strettoi, E. (2003). Neural remodeling in retinal degeneration. *Progress in Retinal and Eye Research, 22*, 607–655.

Marc, R. E., Liu, W. L., Kalloniatis, M., Raiguel, S. F., & van Haesendonck, E. (1990). Patterns of glutamate immunoreactivity in the goldfish retina. *Journal of Neuroscience, 10*(12), 4006–4034.

Marc, R. E., Murry, R. F., & Basinger, S. F. (1995). Pattern recognition of amino acid signatures in retinal neurons. *Journal of Neuroscience, 15*(7 Pt. 2), 5106–5129.

Or, E., David, P., Alla Shainskaya, S., Tal, D. M., & Karlishs, S. J. D. (1993). Effects of competitive sodium-like antagonists on Na,K-ATPase suggest that cation occlusion from the cytoplasmic surface occurs in two steps. *Journal Biological Chemistry, 268*, 16929–16937.

Pang, J. J., Gao, F., & Wu, S. M. (2004). Light-evoked current responses in rod bipolar cells, cone depolarizing bipolar cells and AII amacrine cells in dark adapted mouse retina. *Journal of Physiology, 558*, 897–912.

Petrunkina, A. M., Harrison, R. A. P., Ekhlasi-Hundrieser, M., & Töpfer-Petersen, E. (2004). Role of volume-stimulated osmolyte and anion channels in volume regulation by mammalian sperm. *Molecular and Human Reproduction, 10*, 815–823.

Piletz, J. E., May, P. J., Wang, G., & Zhu, H. (2003). Agmatine crosses the blood–brain barrier. *Annals of New York Academy Sciences, 1009*, 64–74.

Raasch, W., Schafer, U., Chun, J., & Dominiak, P. (2001). Biological significance of agmatine, an endogenous ligand at imidazoline binding sites. *British Journal of Pharmacology, 133*, 755–780.

Rohrer, B., Blanco, R., Marc, R. E., Lloyd, M. B., Bok, D., Schneeweis, D., et al. (2004). Functionally intact glutamate-mediated signaling in bipolar-cells of the Trkb knockout mouse retina. *Visual Neuroscience, 21*, 703–713.

Sakata, Y., Olson, J. K., & Michel, W. C. (2003). Assessment of neuronal maturation and acquisition of functional competence in the developing zebrafish olfactory system. *Methods in Cell Science, 25*, 39–48.

Sokoloff, L., Reivich, M., Kennedy, C., Des Rosiers, M. H., Patlak, C. S., Pettigrew, K. D., et al. (1977). The [14C]deoxyglucose method for the measurement of local cerebral glucose utilization: theory, procedure, and normal values in the conscious and anesthetized albino rat. *Journal of Neurochemistry, 28*, 897–916.

Steullet, P., Cate, H. S., Michel, W. C., & Derby, C. D. (2000). Functional units of a compound nose: aesthetasc sensilla house similar populations of olfactory receptor neurons on the crustacean antennule. *The Journal of Comparative Neurology, 418*, 270–280.

Sun, D., Rait, J. L., & Kalloniatis, M. (2003). Inner retinal neurons display differential responses to *N*-methyl-D-aspartate receptor activation. *The Journal of Comparative Neurology, 465*, 38–56.

Takahashi, D. K., Jones, B. W., Marc, R. E., & K., W. (2004). Excitation mapping in a rodent seizure model. *American Epilepsy Society, 58th Annual Meeting, Abstract 1.040.*

Tasaki, I., Watanabe, A., & Singer, I. (1966). Excitability of squid giant axons in the absence of univalent cations in the external medium. *Proceedings of the National Academy of Sciences of the United States of America, 56*, 1116–1122.

Wässle, H. (2004). Parallel processing in the mammalian retina. *Nature Reviews Neuroscience, 5*, 1–11.

Weininger, D., Weininger, A., & J.L., W. (1989). SMILES. 2. Algorithm for generation of unique SMILES notation. *Journal of Chemical Information and Computer Science, 29*, 97–101.

Yingcharoen, K., Rinvik, E., Storm-Mathisen, J., & Ottersen, O. P. (1989). Gaba, glycine, glutamate, aspartate and taurine in the perihypoglossal nuclei—an immunocytochemical investigation in the cat with particular reference to the issue of amino-acid colocalization. *Experimental Brain Research, 78*(2), 345–357.

Yoshikami, D. (1981). Transmitter sensitivity of neurons assayed by autoradiography. *Science, 212*, 929–930.